Estimation of Maximum Interference-Free Transmit Power Level for Opportunistic Spectrum Access

Brian L. Mark and Ahmed O. Nasif
Dept. of Electrical and Computer Eng.
George Mason University
4400 University Drive, MS 1G5
Fairfax, VA 22030
tel: 703-993-4069, fax: 703-993-1601
email: { bmark , anasif }@gmu.edu

NAPL Technical Report
Number: TR-GMU-NAPL-Y08-N1
Date: August 4, 2008

GMU Network Architecture and Performance Laboratory (NAPL)

Abstract

We consider a scenario in which frequency agile radios opportunistically share a fixed spectrum resource with a set of primary nodes. We develop a collaborative scheme for a group of frequency agile radios to estimate the maximum power at which they can transmit on a given frequency channel, without causing harmful interference to the primary receivers. The proposed scheme relies on signal strength measurements taken by a group of frequency agile radios, which are then used by a target node to characterize the spatial size of its perceived spectrum hole in terms of the maximum permissible transmit power. We derive an approximation to the maximum interference-free transmit power using the Cramér-Rao bound on localization accuracy. We focus on the case of a single transmitter, but briefly discuss how the proposed approach can extend to more general situations with multiple transmitters. We present numerical results to demonstrate the effectiveness of the proposed scheme under a variety of scenarios.

Index Terms

Spectrum access, Spectrum sharing, Cognitive radio, Radio resource management, Collaboration, Geolocation, Cramér-Rao bound

Estimation of Interference-Free Transmit Power for Opportunistic Spectrum Access

Brian L. Mark and Ahmed O. Nasif

I. Introduction

In conventional wireless systems, the spectrum is allocated statically among a set of transmitters over a geographic coverage area. Recent studies have shown that significant portions of the wireless spectrum are highly underutilized [1], [2]. In principle, such "spectrum holes" could be exploited by frequency-agile radios (FARs), which are capable of dynamically tuning to different frequency ranges. Frequency agility and high receiver sensitivity are key features of emerging cognitive radios (CRs) [3], [4]. A group of FARs could exploit the presence of spectrum holes in the allocated spectrum by communicating on frequency channels lying within the holes. An open research question is whether effective opportunistic spectrum sharing can be realized efficiently and practically.

The challenges and potential benefits of opportunistic spectrum sharing have generated considerable research interest in recent years [5], [6]. We mention a few examples of related work in this area. The effect of cooperation among CRs is studied in [7], [8] and is shown to increase the agility and detection probability of the nodes. Information-theoretic and game-theoretic approaches are taken in [9]–[12] to study the achievable capacity of CRs under interference, power, and fairness constraints. Practical challenges in the implementation and hardware design of CRs are addressed in [13] .

In this paper, we focus on the problem of estimating the size of a spectrum hole in terms of the maximum power that a FAR node can transmit on a given frequency channel without causing harmful interference to primary users. In [14], the impact of secondary transmissions on a primary receiver is studied in terms of interference probability. Because of the integral forms involved it is difficult to use the given probability expressions to solve for the allowable secondary transmit power. In [15], an additional *no-talk radius* is defined within which the secondary users must be quiet to guarantee service to primary users within some a *protected radius*. Once these distances are specified (in terms of SNR margins), the aggregate interference at the edge of the protected region is computed, which can then be used to obtain the total permissible secondary transmit power. However, this approach assumes that the primary transmit power and the local SNR at the secondary receivers are already accurately known, so that SNR can be used as a proxy for distance. To avoid these limitations, our approach exploits collaboration among secondary nodes for explicit sensing of the primary transmitter's power and location. We focus on the case of a single transmitter, but briefly discuss how the proposed approach can extend to more general situations.

A basic mechanism for opportunistic spectrum access is the Listen-Before-Talk (LBT) scheme [16]. In the LBT scheme, a FAR node "listens" on a given frequency channel. When the channel is sensed idle, the FAR node has

the opportunity to "talk," i.e., to transmit on the channel for up to a certain maximum duration at a power level not exceeding a fixed threshold. To avoid causing harmful interference to the primary users, the maximum power level and the maximum talk duration in LBT must be chosen relatively conservatively in practice. This can severely limit the potential capacity gains that could be achievable with opportunistic spectrum sharing.

Higher capacity gains could be achieved if the FAR nodes were capable of collaborating and exchanging local information concerning the primary user's transmission characteristics. In [16], a simple collaborative version of LBT was shown to improve the spectrum sharing capacity gain by an order of magnitude. To further improve effectiveness of opportunistic spectrum sharing, signal strength (SS) measurements of the primary user could be shared by FAR nodes and used by a given FAR node to determine the maximum power level at which it can transmit without causing harmful interference to the primary user. We refer to this power level as the maximum interference-free transmit power (MIFTP).

We develop a method to estimate the MIFTP for a given FAR node on a given frequency channel, based on SS measurements collected by one or more FAR nodes in the vicinity of a primary transmitter. The MIFTP characterizes the size of the spectrum hole in the spatial domain with respect to a given FAR node and frequency channel. The SS measurements may be obtained by a single FAR node at different locations at different points in time, or by collaborative sharing of measurement information among spatially separated FAR nodes. We make the conservative assumption that the primary transmitter transmits at constant power during an observation period. Thus, we do not address the separate issue of opportunistic spectrum access in the time-domain, i.e., exploiting periods for which the primary transmitter may be idle [17], [18].

Our proposed approximation for MIFTP is derived from the maximum likelihood estimate of the location of the primary transmitter based on SS measurements and the associated Cramér-Rao bound (CRB) on the error of the estimator. The estimator assumes a lognormal shadowing model of signal propagation. Using the CRB for the location estimator, an estimate for the MIFTP is derived. The canonical localization problem assumes that the transmit power is known. However, in a wireless system with opportunistic spectrum sharing, the secondary users may not have access to this information. Moreover, in some scenarios, the primary transmitter may adjust its transmit power over time. Therefore, we extend the canonical localization problem to incorporate estimation of the transmit power in addition to the position of the primary transmitter. The resulting location estimate is then used to calculate an estimate of the MIFTP, which in general is more conservative than the MIFTP derived from the canonical localization problem.

The remainder of the paper is organized as follows. Section II describes the model and key concepts of opportunistic spectrum sharing used in the paper. Section III describes the canonical SS localization model and

extends the canonical model to the case where the transmit power is unknown. Section IV derives an approximation for the MIFTP. Section V presents numerical results, which demonstrate the effectiveness of the proposed approach to spectrum sharing. Section VI briefly discusses how the proposed approach could be extended to more general situations with multiple transmitters. Finally, the paper is concluded in Section VII. For clarity of exposition we use the following notational conventions: deterministic quantities are in small letters, random variables are in capital letters, estimators are in hats, vectors and matrices are in small and capital bold letters, respectively.

II. Opportunistic Spectrum Sharing

We assume a model of spectrum sharing, whereby a set of FAR nodes attempt to opportunistically make use of unused spectrum, without causing harmful interference to the primary users. The FAR nodes identify and make use of such "spectrum holes" by an opportunistic spectrum access mechanism. In this section, we discuss the concept of opportunistic spectrum access and define a critical parameter called the maximum interference-free transmit power (MIFTP). The MIFTP for a FAR node on a given frequency channel is essentially equivalent to the radius of a spectrum hole in the spatial domain. We then discuss the role of localization in computing the MIFTP.

A. Opportunistic spectrum access

In a noncooperative spectrum sharing environment, a set of users called *cooperative* or *secondary* users, seeks to make use of the spectrum resource, originally allocated to another set of users called *noncooperative* or *primary* users. The *primary* users are called *noncooperative*, since no communication between primary and secondary users are allowed. On the other hand, the *secondary* users are called *cooperative*, because they can exchange information among each other in order to perform collaborative spectrum sensing.Without loss of generality, we shall assume the existence of a common control channel that can be used by the secondary users to exchange control information.[1] The objective of a noncooperative spectrum access scheme is to maximize the utilization of the spectrum resource by providing a means for the secondary users to utilize available spectrum, without causing harmful interference to noncooperative users. By contrast, cooperative spectrum access schemes, such as the family of CSMA protocols, seek to provide fair and efficient spectrum usage among the cooperative users by means of collision sensing or collision avoidance mechanisms.

Listen-Before-Talk (LBT) is a basic scheme for opportunistic spectrum access in a noncooperative environment [16]. A FAR node implementing LBT *listens* to a given frequency channel. When the received power on the channel falls below a threshold η, the FAR node may then use the channel for its own transmission during the *talk*

[1] In practice, any available channel can be used to exchange control information between two secondary users. For example, signal measurements with respect to a frequency channel γ could be exchanged on a different frequency channel ζ.

state. We shall assume that channel contention among the cooperative FAR nodes is resolved using an appropriate medium access control (MAC) protocol. The FAR node that accesses the channel transmits at a signal level not exceeding a certain maximum transmit power s^*. This power level, which we call the maximum interference-free transmit power (MIFTP), may be estimated on the basis of signal measurements obtained during the *listen* state. Under the LBT scheme, the maximum duration of the *talk* phase is limited to a certain value $\tau_{\max}$. The value of $\tau_{\max}$ may be fixed or also estimated based on measurements taken during the *listen* state. The interdependencies of the parameters η, $\tau_{\max}$, and s^* are studied in [16].

In [16], a variation of the basic LBT scheme, called *cooperative LBT*, is considered. In collaborative LBT, a group of FAR nodes share information obtained during their respective listen states. Each FAR node in the group executes the individual LBT scheme. If at least one FAR node in the group detects the presence of a signal from a primary user, then all of the FAR nodes are alerted and revert to the listen state. By collaborative sharing of information, cooperative LBT can achieve significantly higher capacity gains.

In this paper, we take the idea of collaborative spectrum access a step further, by allowing the FAR nodes to share more detailed information obtained from SS measurements. Using such information, the FAR nodes can more accurately estimate the MIFTP values that limit their respective transmit powers during the talk state. In particular, the FAR nodes share SS measurements, as well as their own locations, with each other. It is assumed that the FAR nodes know their own locations via GPS (Global Positioning System) or some type of self-localization scheme (cf. [19]–[22]).

B. Maximum interference-free transmit power

Next, we provide a formal definition for the MIFTP. Consider a FAR node a and a primary transmitter p, which transmits on a given frequency channel γ. We define a spectrum hole with respect to γ for the FAR node a in terms of the maximum power at which the node a can transmit without causing harmful interference to any potential primary receiver or victim node v, within the range of the primary transmitter p. This maximum power level, called the MIFTP, is defined more precisely as the maximum transmit power of node a on a *target frequency channel* γ, such that the probability of interference to any victim node v is less than a prescribed threshold (cf. [16]).

We shall assume that all transmissions are omnidirectional and the signal propagation is governed by a lognormal shadowing model (cf. [23]). Hence, the propagation loss between two nodes i and j can be expressed as

$$L_{i,j} = g(d_{i,j}, \epsilon_{i,j}) + W, \tag{1}$$

where the function $g(d, \epsilon)$, represents the path loss component, with ϵ denoting the path loss factor. Although in practice, $\epsilon_{i,j}$ depends on the specific propagation condition between nodes i and j (for example, line-of-sight versus

non-line-of-sight, indoor versus outdoor, urban versus rural, etc.), throughout this work we shall assume that $\epsilon_{i,j}$ is a fixed known constant, i.e., $\epsilon_{i,j} = \epsilon$. For simplicity, we assume that $g(d, \epsilon) = 10\epsilon \log_{10} d$ and denote it by $g(d)$. More complicated path loss models could be incorporated into our analysis, such as the empirical propagation model (EPM-73) [24], Longley-Rice model [25], or the TIREM (Terrain Integrated Rough Earth Model) [26]. In fact, this would be necessary for practical systems, since the different links involved (primary-primary, primary-secondary, secondary-secondary) are not homogeneous. But here, without loss of generality, we adopt the generic path loss model to focus on the issue of MIFTP estimation, and our results can be applied to real systems as long as a valid propagation model is used.

We assume that the shadowing noise is a zero mean, Gaussian random variable $W \sim \mathcal{N}(0, \sigma_W^2)$. The received power at node v due to node p is given by

$$R_v = s_p - L_{p,v} = s_p - g(d_{p,v}) + W, \tag{2}$$

where s_p is the transmit power of node p. The received power at node v from node a is given by

$$I_v = s_a - L_{a,v} = s_a - g(d_{a,v}) + W, \tag{3}$$

where s_a is the transmit power of a. Our spectrum sharing model is based on the following definitions.

Definition 1: The *outage probability* of a victim node v with respect to the transmitter p, is the probability that the received power R_v from node p is below a predefined detection threshold r_{min}:

$$P_{\text{out}}(p, v) \triangleq P\left\{R_v < r_{\text{min}}\right\}, \tag{4}$$

when p is transmitting. In general, r_{min} is determined by the primary receiver's structure, noise statistics and QoS.

Definition 2: The *coverage distance* is the maximum distance between the node p and any potential victim node v such that the outage probability does not exceed a predefined threshold $\varepsilon_{\text{cov}} > 0$:

$$d_{\text{cov}}(p) \triangleq \max\left\{d_{p,v} : P_{\text{out}}(p, v) \leq \varepsilon_{\text{cov}}\right\} = g^{-1}\left(s_p - r_{\text{min}} + \sigma_W Q^{-1}(1 - \varepsilon_{\text{cov}})\right), \tag{5}$$

where $g^{-1}(\cdot)$ denotes the inverse of $g(\cdot)$ and $Q(x) \triangleq \frac{1}{\sqrt{2\pi}} \int_x^\infty e^{-\frac{t^2}{2}} dt$ denotes the standard Q-function.
Note that $d_{\text{cov}}(p)$ depends on s_p, r_{min}, ε_{cov}, σ_W^2 and the path loss function $g(\cdot)$. We assume that the FAR node knows or can estimate s_p and therefore can evaluate $d_{\text{cov}}(p)$.

Definition 3: The circle centered at node p with radius $d_{\text{cov}}(p)$ is the *coverage area* of the transmitter p.
Any potential victim node v, which lies outside of coverage area of node p would be oblivious to the interference caused by the FAR node a.

Definition 4: The *interference probability* with respect to a given victim node v is the probability that I_v exceeds a predefined interference tolerance threshold $i_{\max}$:

$$P_{\text{int}}(a, v) \triangleq \Pr\{I_v \geq i_{\max}\}, \tag{6}$$

when node a is transmitting. This threshold can be set to meet the primary system's interference tolerance policy. Under the lognormal shadowing model (1), the interference probability is given by

$$P_{\text{int}}(a, v) = Q\left(\frac{i_{\max} - s_a + g(d_{a,v})}{\sigma_W}\right). \tag{7}$$

Definition 5: For a fixed primary transmitter p and FAR node a, the ***MIFTP*** is the maximum transmit power of the FAR node such that the interference probability with respect to any potential victim node within the coverage distance from node p does not exceed a threshold $\varepsilon_{\text{int}} > 0$:

$$s_a^* \triangleq \max\{s_a : P_{\text{int}}(a, v) \leq \varepsilon_{\text{int}}, \forall v : d_{p,v} \leq d_{\text{cov}}(p)\}. \tag{8}$$

Alternatively, the MIFTP can be defined in terms of the worst-case interference probability:

$$P_{\text{int}}(a) = \sup_v P_{\text{int}}(a, v) = Q\left(\frac{i_{\max} - s_a + g(d_a^*)}{\sigma_W}\right), \tag{9}$$

where $d_a^* \triangleq d_{p,a} - d_{\text{cov}}(p)$ is called the *critical distance* for the FAR node a with respect to the primary transmitter p and the supremum is taken over all potential victim nodes v such that $d_{p,v} \leq d_{\text{cov}}(p)$. Then

$$s_a^* = \max\{s_a : P_{\text{int}}(a) \leq \varepsilon_{\text{int}}\}.$$

Proposition 1: The MIFTP is given by[2]

$$s_a^* = \begin{cases} i_{\max} + g(d_a^*) - \sigma_W Q^{-1}(\varepsilon_{\text{int}}), & \text{if } d_{p,a} > d_{\text{cov}}(p), \\ -\infty, & \text{otherwise.} \end{cases} \tag{10}$$

Proof: If the FAR node a lies within the coverage area of node p, i.e., if $d_{p,a} \leq d_{\text{cov}}$, a victim node v can be placed arbitrarily close to node a within the coverage area. Hence, there is no positive value of s_a at which the FAR node could transmit without causing harmful interference to potential victim nodes lying within the coverage area. This implies that the MIFTP, s_a^*, is zero in this case.

If the FAR node lies outside the coverage area of node p (see Fig. 1), then $d_{p,a} > d_{\text{cov}}(p)$. In this case, the minimum distance to a potential victim node lying within the coverage area is given by

$$d_a^* = d_{p,a} - d_{\text{cov}}(p).$$

[2]When $s_a^* = -\infty$, the FAR node should not attempt to transmit on the target frequency channel.

To avoid causing harmful interference to victim nodes lying within the coverage area of node p, the transmit power, s_a, of the FAR node a must be such that the condition in (8) is satisfied. Using (3), we find that this is equivalent to requiring that

$$s_a \leq i_{\max} + g(d_a^*) - \sigma_W Q^{-1}(\varepsilon_{\text{int}}). \tag{11}$$

■

C. Role of localization

Our proposed scheme for discovering spectrum holes is based on localizing the primary transmitters and using the location estimates to approximate the MIFTP. Localization in this context differs from more conventional scenarios (cf. [27]) in two respects: (1) The FAR nodes collaboratively localize the primary transmitter. (2) No cooperation is assumed between the FAR node and the primary transmitter. For the purpose of spectrum hole estimation, localization techniques based on the SS and angle-of-arrival (AOA) information are more appropriate than time-of-arrival (TOA) or time-difference-of-arrival (TDOA) methods. This is because in the noncooperative scenario, knowledge of the transmit waveform, which is required to extract the TOA information, is typically not available or difficult to obtain. For TDOA estimation, the conventional generalized cross-correlation method can be very demanding. This is because even for a single TDOA estimate, the received (digitized) signals at two nodes need to be transmitted to a common site for processing, [28] p. 54. Since antenna arrays needed to collect AOA measurements, are expensive and can be difficult to deploy, we only consider location estimation using SS in this paper.

III. Signal Strength-based Localization

A. Canonical Signal Strength Model

Let P_T denote the total signal power received at a FAR node located at position (x, y). Let (x_p, y_p) denote the location of the primary transmitter. The total received signal power consists of two components:

$$P_T = P_r + P_n, \tag{12}$$

where P_r is the received signal power from the primary transmitter and P_n denotes the noise power. The noise power P_n is primarily due to thermal noise power at the receiver, which generally does not depend on the location of the receiver. Even if other sources of noise are present, it is reasonable to assume that the total noise power P_n is constant for short periods of time and hence can be estimated in advance. Therefore, we shall assume that the signal power P_r in (12) can be obtained directly from measurements.

The signal power P_r can be modeled as follows:

$$P_r = k10^{\frac{s_p}{10}} \frac{G^2\Gamma}{d^\epsilon}, \tag{13}$$

where s_p is the transmitted power from the primary transmitter (measured in dBW or dBm), $d = \sqrt{(x-x_p)^2 + (y-y_p)^2}$ is the distance between the transmitter and the FAR node, ϵ is the path loss factor, G is a random variable that captures the effect of multipath or fast fading, Γ is a random variable that captures the effect of shadowing or slow fading, and k is given by $k = \frac{g_t g_r}{4\pi}$, where g_t and g_r are the antenna gains of the transmitter and receiver, respectively. The fast fading parameter G is modeled either as a Rayleigh or as a Rician random variable, while the slow fading parameter Γ is modeled by a lognormal distribution. In units of dBW, (13) can be written as:

$$P_r = z + \kappa + 10\log_{10}\Gamma + 10\log_{10} k, \tag{14}$$

where $z = s_p - 10\epsilon\log_{10} d$ and $\kappa = 20\log_{10} G$. The fast fading term κ varies in time on a short time-scale. By averaging the received power over a given time interval, the time-averaged version of (14) can be written as

$$\overline{P}_r = z + \bar{\kappa} + 10\log_{10}\Gamma + 10\log_{10} k, \tag{15}$$

where $\bar{\kappa}$ is the time-average of the fast fading component κ.

Let us assume that the transmitter power s_p, the time-averaged fast fading component $\bar{\kappa}$, the term $E[10\log_{10}\Gamma] + 10\log_{10} k$, and the path loss factor ϵ are known. The basic observation equation for SS-based localization can then be written as follows:

$$S = z + W, \tag{16}$$

where the "observed" signal strength S is defined by

$$S \triangleq \overline{P}_r - \bar{\kappa} - E[10\log_{10}\Gamma] - 10\log_{10} k, \tag{17}$$

and W is a zero-mean Gaussian random variable with variance $\sigma_W^2 = \text{Var}[10\log_{10}\Gamma]$.

We assume that the location and transmit power of the primary transmitter is constant during an observation period. Now suppose that a set of uncorrelated observed SS measurements, $\{S_1, \cdots, S_N\}$, is available, together with a corresponding set of position coordinates $\{\boldsymbol{L}_1, \cdots, \boldsymbol{L}_N\}$, where $\boldsymbol{L}_i = [x_i, y_i]^T$, $i = 1, \cdots, N$. The set of observables,

$$\mathcal{O} \triangleq \{(S_i, \boldsymbol{L}_i) : i = 1, \cdots, N\},$$

may be obtained in several ways. For example, consider a scenario in which N FAR nodes, located at positions $\boldsymbol{L}_1, \cdots, \boldsymbol{L}_N$, collect the SS observables $S_1, \cdots, S_N$ at a given observation window. The FAR nodes exchange their observables among each other, such that at least one of the FAR nodes receives the entire set $\mathcal{O}$. Such a FAR

node can then compute an estimate $\hat{\boldsymbol{L}} = [\hat{X}_p, \hat{Y}_p]^T$ of the location of the primary transmitter. Alternatively, the observable set $\mathcal{O}$ may be obtained by measurements from a single FAR node at N different points in time along a trajectory as the node moves in the coverage area. In general, a given observable $(S_i, \boldsymbol{L}_i)$ may be obtained either from a measurement taken by the FAR node itself in the past, or from a measurement by another FAR node, which shares this information with the given FAR node.

Given a set of observations, $\mathcal{O}$, the observation equations can be written in vector form as follows:

$$\boldsymbol{S} = \boldsymbol{z} + \boldsymbol{W}, \tag{18}$$

where

$$\boldsymbol{S} = [S_1, \cdots, S_N]^T, \ \boldsymbol{z} = [z_1, \cdots, z_N]^T, \ \boldsymbol{W} = [W_1, \cdots, W_N]^T, \tag{19}$$

with

$$z_i = s_p - 10\epsilon \log_{10} d_i \text{ and } d_i = \sqrt{(x_i - x_p)^2 + (y_i - y_p)^2}. \tag{20}$$

It will be convenient to define $\boldsymbol{d} = [d_1, \cdots, d_N]^T$, such that $\boldsymbol{z} = s_p \mathbf{1} - 10\epsilon \log_{10} \boldsymbol{d}$, where $\mathbf{1}$ is a $N \times 1$ vector of all ones. An estimate $\hat{\boldsymbol{L}}$ of the location of the primary transmitter can be obtained from the SS observation equation (18).

B. Cramér-Rao bound

The CRB provides a lower bound on the variance (or covariance matrix) of any unbiased estimate of an unknown parameter. For the SS localization model of (18) , the CRB of any unbiased estimate $\hat{\boldsymbol{L}}$ of $\boldsymbol{L}$ is given by

$$E_{\boldsymbol{L}}[(\hat{\boldsymbol{L}} - \boldsymbol{L})(\hat{\boldsymbol{L}} - \boldsymbol{L})^T] \geq \boldsymbol{J}_{\boldsymbol{L}}^{-1}, \tag{21}$$

where $E_{\boldsymbol{L}}[\cdot]$ denotes conditional expectation with respect to $\boldsymbol{L}$ and $\boldsymbol{J}_{\boldsymbol{L}}$ is the Fisher information matrix (FIM) given by

$$\boldsymbol{J}_{\boldsymbol{L}} = E_{\boldsymbol{L}} \left[\frac{\partial}{\partial \boldsymbol{L}} \ln f_{\boldsymbol{S}|\boldsymbol{L}}(\boldsymbol{S}) \left(\frac{\partial}{\partial \boldsymbol{L}} \ln f_{\boldsymbol{S}|\boldsymbol{L}}(\boldsymbol{S}) \right)^T \right], \tag{22}$$

where $f_{\boldsymbol{S}|\boldsymbol{L}}(\boldsymbol{S})$ is the likelihood function. In (21), the matrix inequality $\boldsymbol{A} \geq \boldsymbol{B}$ should be interpreted as the assertion that the matrix $\boldsymbol{A} - \boldsymbol{B}$ is non-negative definite. The CRB provides a lower bound on the mean-squared errors for the components of $\boldsymbol{L}$.

The FIM can be expressed as follows:

$$\boldsymbol{J}_{\boldsymbol{L}} = \left(\frac{10\epsilon}{\sigma_W \ln 10} \right)^2 \boldsymbol{H} \boldsymbol{D}^2 \boldsymbol{H}^T, \tag{23}$$

where

$$\boldsymbol{H} \triangleq \begin{bmatrix} \cos\phi_1 & \cos\phi_2 & \cdots & \cos\phi_N \\ \sin\phi_1 & \sin\phi_2 & \cdots & \sin\phi_N \end{bmatrix}, \tag{24}$$

$$\boldsymbol{D} \triangleq \text{diag}\left[d_1^{-1}, \cdots, d_N^{-1}\right], \tag{25}$$

and

$$\phi_i = \tan^{-1}\left(\frac{y_p - y_i}{x_p - x_i}\right), \quad i = 1, \cdots, N, \tag{26}$$

is the angle between x-axis and the line connecting (x_i, y_i) and (x_p, y_p), measured counterclockwise. Here diag$[\cdot]$ denotes a diagonal matrix. The expression (23) can be derived by essentially following the derivation of FIM given in [27] for TOA-based localization.

The CRB $\boldsymbol{J}_{\boldsymbol{L}}^{-1}$ provides a lower bound on the mean squared error (MSE) of the unbiased estimate $\hat{\boldsymbol{L}} = [\hat{X}_p, \hat{Y}_p]^T$. We denote this quantity as $\mathcal{E}_{\hat{\boldsymbol{L}}}(\boldsymbol{L})$, which can be expressed in closed-form:

$$\mathcal{E}_{\hat{\boldsymbol{L}}}(\boldsymbol{L}) = \frac{2\left(\frac{\sigma_W \ln 10}{10\epsilon}\right)^2 \sum_{i=1}^{N} d_i^{-2}}{\sum_{i=1}^{N}\sum_{j=1}^{N} d_i^{-2} d_j^{-2} \sin^2(\phi_i - \phi_j)}. \tag{27}$$

We write $\mathcal{E}_{\hat{\boldsymbol{L}}}(\boldsymbol{L})$ to denote the lower bound on the MSE of $\hat{\boldsymbol{L}}$ as a function of $\boldsymbol{L}$. It can be shown (cf. [27], [29]) that the CRB is achieved by the maximum likelihood estimator (MLE) asymptotically as $\sigma_W^2 \to 0$. We denote the MLE by $\hat{\boldsymbol{L}}_{\text{ML}}$.

C. Unknown Transmit Power

Up to this point, we have assumed that the transmit power s_p of the primary transmitter is known. In reality, s_p is more likely to be unknown, since no cooperation between the FAR node and the primary transmitter is assumed. In the *noncooperative* localization scenario, in addition to s_p, the antenna parameters of the transmitter are treated as unknowns. We lump all of these unknown parameters into s_p, such that s_p represents the model uncertainty due to the transmitter characteristics, instead of representing just the transmit power [30]. The key parameters of the propagation environment, namely, ϵ and σ_W, may also be treated as unknowns and can be estimated separately [31], [32]. For the ease of exposition and in order to focus on the localization issue, we treat the transmit power as the only unknown quantity of the model besides the transmitter location. In this section, we assume that s_p is a deterministic unknown quantity which is to be estimated by the FAR node along with the primary transmitter's location $\boldsymbol{L} = [x_p, y_p]^T$. The parameter vector of interest and its estimator are denoted by

$$\boldsymbol{\Theta} = [x_p, y_p, s_p]^T \text{ and } \hat{\boldsymbol{\Theta}} = [\hat{X}_p, \hat{Y}_p, \hat{S}_p]^T,$$

respectively.

Next, we show that for the SS model of (18), the MLE of $\boldsymbol{\Theta}$ can be approximated as an unbiased estimate that achieves the CRB under certain conditions. The CRB for $\boldsymbol{\Theta}$ is given by

$$E_{\boldsymbol{\Theta}}[(\boldsymbol{\Theta}-\hat{\boldsymbol{\Theta}})(\boldsymbol{\Theta}-\hat{\boldsymbol{\Theta}})^T] \geq \boldsymbol{J}_{\boldsymbol{\Theta}}^{-1},$$

where the FIM $\boldsymbol{J}_{\boldsymbol{\Theta}}$ is defined as

$$\boldsymbol{J}_{\boldsymbol{\Theta}} = E_{\boldsymbol{\Theta}}\left[\frac{\partial}{\partial \boldsymbol{\Theta}} \ln f_{\boldsymbol{S}|\boldsymbol{\Theta}}(\boldsymbol{S}) \left(\frac{\partial}{\partial \boldsymbol{\Theta}} \ln f_{\boldsymbol{S}|\boldsymbol{\Theta}}(\boldsymbol{S})\right)^T\right], \tag{28}$$

and $f_{\boldsymbol{S}|\boldsymbol{\Theta}}(\boldsymbol{S})$ denotes the likelihood function.

The next proposition gives a closed-form expression for the FIM, analogous to (23).

Proposition 2: The FIM is given by

$$\boldsymbol{J}_{\boldsymbol{\Theta}} = \frac{1}{\sigma_W^2}\boldsymbol{B}\boldsymbol{G}\boldsymbol{D}^2\boldsymbol{G}^T\boldsymbol{B}, \tag{29}$$

where $\boldsymbol{D}$ is given by (25),

$$\boldsymbol{B} \triangleq \text{diag}\left[\frac{-10\epsilon}{\ln 10}, \frac{-10\epsilon}{\ln 10}, 1\right], \tag{30}$$

$$\boldsymbol{G} \triangleq \begin{bmatrix} \cos\phi_1 & \cdots & \cos\phi_N \\ \sin\phi_1 & \cdots & \sin\phi_N \\ d_1 & \cdots & d_N \end{bmatrix}. \tag{31}$$

A proof of (29) is given in Appendix A.

By multiplying out the matrices in (29) we can rewrite the FIM as

$$\boldsymbol{J}_{\boldsymbol{\Theta}} = \begin{bmatrix} \boldsymbol{J}_{\boldsymbol{L}} & \boldsymbol{a} \\ \boldsymbol{a}^T & \frac{N}{\sigma_W^2} \end{bmatrix}, \tag{32}$$

where $\boldsymbol{J}_{\boldsymbol{L}}$ denotes the FIM as defined in (23) and

$$\boldsymbol{a} \triangleq -\frac{10\epsilon}{\sigma_W^2 \ln 10}\left[\sum_{i=1}^{N}\frac{\cos\phi_i}{d_i}, \sum_{i=1}^{N}\frac{\sin\phi_i}{d_i}\right]^T.$$

Using the matrix inversion formula (see [33], p. 33), we have

$$\boldsymbol{J}_{\boldsymbol{\Theta}}^{-1} = \begin{bmatrix} \boldsymbol{J}_{\boldsymbol{L}}^{-1} + b^{-1}\boldsymbol{c}\boldsymbol{c}^T & -b^{-1}\boldsymbol{c} \\ -b^{-1}\boldsymbol{c}^T & b^{-1} \end{bmatrix}, \tag{33}$$

where

$$b \triangleq \frac{N}{\sigma_W^2} - \boldsymbol{a}^T\boldsymbol{J}_{\boldsymbol{L}}^{-1}\boldsymbol{a} \tag{34}$$

and $\boldsymbol{c} \triangleq \boldsymbol{J}_{\boldsymbol{L}}^{-1}\boldsymbol{a}$, assuming that $\boldsymbol{J}_{\boldsymbol{L}}^{-1}$ exists. From $\boldsymbol{J}_{\boldsymbol{\Theta}}^{-1}$ we can get lower bounds on the MSE of the primary transmitter's transmit power and position. We denote these two quantities as $\mathcal{E}_{\hat{S}_p}(\boldsymbol{\Theta})$ and $\mathcal{E}_{\hat{\boldsymbol{L}}}(\boldsymbol{\Theta})$, respectively, where

$$\mathcal{E}_{\hat{S}_p}(\boldsymbol{\Theta}) = \left[\boldsymbol{J}_{\boldsymbol{\Theta}}^{-1}\right]_{(3,3)} = b^{-1}, \tag{35}$$

and

$$\mathcal{E}_{\hat{\boldsymbol{L}}}(\boldsymbol{\Theta}) = \left[\boldsymbol{J}_{\boldsymbol{\Theta}}^{-1}\right]_{(1,1)} + \left[\boldsymbol{J}_{\boldsymbol{\Theta}}^{-1}\right]_{(2,2)} = \mathrm{Tr}(\boldsymbol{J}_{\boldsymbol{L}}^{-1} + b^{-1}\boldsymbol{c}\boldsymbol{c}^T) = \mathcal{E}_{\hat{\boldsymbol{L}}}(\boldsymbol{L}) + \mathcal{E}_{\hat{S}_p}(\boldsymbol{\Theta})\mathrm{Tr}(\boldsymbol{c}\boldsymbol{c}^T), \tag{36}$$

where $\mathcal{E}_{\hat{\boldsymbol{L}}}(\boldsymbol{L})$ denotes the lower bound on the MSE of the primary transmitter's position estimate given in (27).

We note that for any non-zero $\boldsymbol{a}$, $\mathrm{Tr}(\boldsymbol{c}\boldsymbol{c}^T) > 0$. Therefore, $\mathcal{E}_{\hat{\boldsymbol{L}}}(\boldsymbol{\Theta}) > \mathcal{E}_{\hat{\boldsymbol{L}}}(\boldsymbol{L})$ and the position estimation accuracy degrades by $\mathcal{E}_{\hat{S}_p}(\boldsymbol{\Theta})\mathrm{Tr}(\boldsymbol{c}\boldsymbol{c}^T)$. Since estimating more parameters can only increase the bound on the variance (cf. [34], p. 232), this is the price we pay for estimating the extra parameter s_p. We write $\mathcal{E}_{\hat{S}_p}(\boldsymbol{\Theta})$ and $\mathcal{E}_{\hat{\boldsymbol{L}}}(\boldsymbol{\Theta})$ to denote the lower bound on the MSE of $\hat{S}_p$ and $\hat{\boldsymbol{L}}$, respectively, given as a function of $\boldsymbol{\Theta}$.

Proposition 3: For sufficiently small σ_W,

$$f_{\hat{\boldsymbol{\Theta}}|\boldsymbol{\Theta}}(\hat{\boldsymbol{\Theta}}) \propto \exp\left\{-\frac{1}{2}(\hat{\boldsymbol{\Theta}} - \boldsymbol{\Theta})^T \boldsymbol{J}_{\boldsymbol{\Theta}}(\hat{\boldsymbol{\Theta}} - \boldsymbol{\Theta})\right\}, \tag{37}$$

which shows that $\hat{\boldsymbol{\Theta}}$ is a multivariate Gaussian random variable with mean $E_{\boldsymbol{\Theta}}[\hat{\boldsymbol{\Theta}}] = \boldsymbol{\Theta}$.

A proof is given in Appendix B.

In Appendix C, we show that

$$\frac{\partial}{\partial \boldsymbol{\Theta}} \ln f_{\boldsymbol{S}|\boldsymbol{\Theta}}(\boldsymbol{S}) = \boldsymbol{J}_{\boldsymbol{\Theta}}(\hat{\boldsymbol{\Theta}} - \boldsymbol{\Theta}), \tag{38}$$

i.e., the estimation error vector is a linear function of the score function $\frac{\partial}{\partial \boldsymbol{\Theta}} \ln f_{\boldsymbol{S}|\boldsymbol{\Theta}}(\boldsymbol{S})$. Assuming that an unbiased estimate exists, a well-known result in estimation theory [35] allows us to conclude that the CRB is achieved by the MLE, which we denote by $\hat{\boldsymbol{\Theta}}_{\mathrm{ML}}$. Since an unbiased estimate exists for sufficiently small shadowing noise variance, we can conclude that the CRB is achieved by $\hat{\boldsymbol{\Theta}}_{\mathrm{ML}}$ asymptotically, as $\sigma_W^2 \to 0$.

IV. Approximation for MIFTP

The true MIFTP, as given in Proposition 1, cannot be calculated directly, since the true location, $\boldsymbol{L} = [x_p, y_p]^T$, of the primary transmitter p is unknown. In this section, we derive an approximation for the MIFTP for the case when the transmit power is known as well as the case in which it is unknown.

A. Known transmit power

Assume first that the transmit power s_p of the primary transmitter is a known constant. Let $\hat{\boldsymbol{L}}_{\mathrm{ML}} = [\hat{X}_p, \hat{Y}_p]^T$ denote the MLE of $\boldsymbol{L}$. Given a set of $N \geq 3$ independent SS measurements from the primary transmitter, obtained

by the FAR nodes, $\hat{\boldsymbol{L}}_{\mathrm{ML}}$ provides an unbiased estimate of $\boldsymbol{L}$ as the shadowing noise tends to zero; i.e., $\hat{\boldsymbol{L}}_{\mathrm{ML}}$ is asymptotically *efficient* as $\sigma_W^2 \to 0$. As discussed in Section III-B, in this asymptotic regime, the mean squared error of $\hat{\boldsymbol{L}}_{\mathrm{ML}}$ achieves the CRB, which we denote by $\boldsymbol{J}_{\boldsymbol{L}}^{-1}$.

Suppose that the FAR node a is located at $\boldsymbol{L}_a = [x_a, y_a]^T$. Given $\hat{\boldsymbol{L}}_{\mathrm{ML}}$, the MLE for the distance $d_{p,a}$, denoted by $\hat{D}_{p,a}$, can be obtained by applying the invariance principle (cf. [34], p. 217), which states that the MLE of a function $h(\cdot)$ of $\boldsymbol{L}$ is given by $h(\hat{\boldsymbol{L}})$, where $\hat{\boldsymbol{L}}$ denotes the MLE of $\boldsymbol{L}$. Hence, we obtain

$$\hat{D}_{p,a} = \sqrt{\left(\hat{X}_p - x_a\right)^2 + \left(\hat{Y}_p - y_a\right)^2}. \tag{39}$$

Proposition 4: In the asymptotic regime $\sigma_W^2 \to 0$, the MLE $\hat{D}_{p,a}$ achieves the associated CRB, given by

$$J_{p,a}^{-1} \triangleq \boldsymbol{H}_{p,a}^T \boldsymbol{J}_{\boldsymbol{L}}^{-1} \boldsymbol{H}_{p,a}, \tag{40}$$

where

$$\boldsymbol{H}_{p,a} \triangleq [\cos\phi_{p,a},\ \ \sin\phi_{p,a}]^T,\ \ \phi_{p,a} = \tan^{-1}\left(\frac{y_p - y_a}{x_p - x_a}\right).$$

A proof is given in Appendix D.

Let $E_{p,a} \triangleq \hat{D}_{p,a} - d_{p,a}$ denote the estimation error of $\hat{D}_{p,a}$. Proposition 4 implies that in the asymptotic regime $\sigma_W^2 \to 0$, $E_{p,a}$ is Gaussian with zero mean and variance $J_{p,a}^{-1}$, i.e.,

$$E_{p,a} \sim \mathcal{N}\left(0, J_{p,a}^{-1}\right). \tag{41}$$

Define $\beta \triangleq \hat{D}_{p,a} - d_{\mathrm{cov}}(p)$. Suppose $E_{p,a} = r$. If $|r| \geq \beta > 0$, then in the worst case, the FAR node lies within $d_{\mathrm{cov}}(p)$ of the true primary transmitter p (see Fig. 2(a)). In this scenario, the FAR node must not transmit, i.e., $s_a^* = -\infty$, to avoid potentially harmful interference to the victim nodes. If $0 < |r| < \beta$, then the FAR can transmit with positive power, i.e., $s_a^* \neq -\infty$ (see Fig. 2(b)).

Proposition 5: Under the assumption (41) and for $|r| \leq 0.993\beta$, the interference probability conditioned on $E_{p,a}$ is upper bounded as follows:

$$P_{\mathrm{int}}(a, v | E_{p,a} = r) \leq Q(b_1 + b_2|r|), \tag{42}$$

where

$$b_1 \triangleq \frac{i_{\max} + 10\epsilon\log_{10}\beta - s_a}{\sigma_W},\ \ b_2 \triangleq -\frac{50\epsilon}{\beta\sigma_W \ln 10}. \tag{43}$$

A proof is given in Appendix E.

Requiring that $s_a \neq -\infty$, we obtain

$$P_{\text{int}}(a,v) = \int_{-\beta}^{\beta} P_{\text{int}}(a,v|E_{p,a}=r) f_{E_{p,a}}(r) dr,$$

where $f_{E_{p,a}}(r)$ denotes the probability density function (pdf) of $E_{p,a}$. We can then show that

$$P_{\text{int}}(a,v) \leq \int_{-\infty}^{\infty} Q(b_1+b_2 r) \frac{1}{\sqrt{2\pi J_{p,a}^{-1}}} \exp\left\{-\frac{r^2}{2J_{p,a}^{-1}}\right\} dr = Q\left(\frac{b_1}{\sqrt{1+b_2^2 J_{p,a}^{-1}}}\right),$$

where the last equality can be found in [36], p. 102.

To obtain an expression for the MIFTP, we require the FAR node transmitter power, s_a, to satisfy

$$Q\left(\frac{b_1}{\sqrt{1+b_2^2 J_{p,a}^{-1}}}\right) \leq \varepsilon_{\text{int}},$$

which implies

$$s_a \leq i_{\max} + 10\epsilon \log_{10}\beta - \sigma_W \sqrt{1+\left(\frac{50\epsilon}{\beta\sigma_W \ln 10}\right)^2 J_{p,a}^{-1}} \cdot Q^{-1}(\varepsilon_{\text{int}}). \tag{44}$$

The right-hand side of (44) provides an approximation for the MIFTP, but since the true CRB of $\hat{D}_{p,a}$, i.e., $J_{p,a}^{-1}$ is unknown, we replace it with the MLE of $J_{p,a}^{-1}$, which is denoted by $\hat{J}_{p,a}^{-1}$. This is justified by the invariance principle mentioned earlier and also illustrated in Section V in our numerical studies.

Recall that for $s_a^* \neq -\infty$, we require that a particular realization of the random variable $E_{p,a} = r$, satisfy the worst case scenario $0 < |r| < \beta$. Since we do not know r, we can only ensure that for $\beta > 0$, the event $(|E_{p,a}| < \beta)$ is satisfied with high probability. Particularly, for $s_a^* \neq -\infty$ and $\varepsilon > 0$ (close to 1), we require $\beta > \beta^* > 0$, where

$$\beta^* \triangleq \min\left\{\tilde{\beta} : \Pr(|E_{p,a}| < \tilde{\beta}) \geq \varepsilon\right\} \tag{45}$$

$$= \sqrt{J_{p,a}^{-1}} \cdot Q^{-1}\left(\frac{1-\varepsilon}{2}\right). \tag{46}$$

For example, for $\varepsilon = 0.9973$, $\beta^* \approx 3\sqrt{J_{p,a}^{-1}}$. Again as before, we replace $J_{p,a}^{-1}$ by $\hat{J}_{p,a}^{-1}$, i.e., we have $\hat{\beta}^* = \sqrt{\hat{J}_{p,a}^{-1}} \cdot Q^{-1}\left(\frac{1-\varepsilon}{2}\right)$. A derivation of (46) is given in Appendix F.

Hence, we obtain the following approximation for the MIFTP:

$$\hat{s}_a = \begin{cases} i_{\max} + 10\epsilon \log_{10}\beta - \sigma_W \sqrt{1+\left(\frac{50\epsilon}{\beta\sigma_W \ln 10}\right)^2 \hat{J}_{p,a}^{-1}} \cdot Q^{-1}(\varepsilon_{\text{int}}), & \text{if } \beta > \hat{\beta}^* > 0 \\ -\infty, & \text{otherwise.} \end{cases} \tag{47}$$

We point out that as the accuracy of the estimate $\hat{D}_{p,a}$ improves, the CRB estimate $\hat{J}_{p,a}^{-1}$ tends to zero and the right-hand side of (47) converges to the true MIFTP as given in (10). The approximate formula (47) for MIFTP requires at least three independent SS measurements, i.e., $N \geq 3$, which should be obtained from FAR nodes in the vicinity of the primary transmitter.

B. Unknown transmit power

If the primary transmitter power s_p is unknown, it can be estimated together with the location $\boldsymbol{L}$ as a parameter vector $\boldsymbol{\Theta} = [\boldsymbol{L}, s_p]$, as discussed in Section III-C. From that section, we know that the MLE, $\hat{\boldsymbol{\Theta}}_{\mathrm{ML}}$, achieves the CRB asymptotically as $\sigma_W^2 \to 0$. Note that, since $d_{\mathrm{cov}}(p)$ depends on s_p (cf. (5)), in this case we need to estimate $d_{\mathrm{cov}}(p)$ as well. Hence it is convenient to work in terms of $\widetilde{\boldsymbol{\Theta}} \triangleq [d_{p,a} \;\; d_{\mathrm{cov}}(p)]^T$ and its associated CRB $\boldsymbol{J}_{\widetilde{\boldsymbol{\Theta}}}^{-1}$, instead of $\boldsymbol{\Theta}$ and its associated CRB $\boldsymbol{J}_{\boldsymbol{\Theta}}^{-1}$. Invoking the invariance principle again, we have $\hat{\widetilde{\boldsymbol{\Theta}}}_{\mathrm{ML}} = [\hat{D}_{p,a} \quad \hat{D}_{\mathrm{cov}}(p)]^T$, where $\hat{D}_{p,a} = \sqrt{\left(\hat{X}_p - x_a\right)^2 + \left(\hat{Y}_p - y_a\right)^2}$ and $\hat{D}_{\mathrm{cov}}(p) = g^{-1}(\hat{S}_p - r_{\min} + \sigma_W Q^{-1}(1 - \varepsilon_{\mathrm{cov}}))$.

Define $E_1 \triangleq E_{p,a} - E_{\mathrm{cov}}$, where $E_{p,a} \triangleq \hat{D}_{p,a} - d_{p,a}$ and $E_{\mathrm{cov}} \triangleq \hat{D}_{\mathrm{cov}}(p) - d_{\mathrm{cov}}(p)$.

Proposition 6: In the asymptotic regime $\sigma_W \to 0$, E_1 can be modeled as $E_1 \sim \mathcal{N}\left(0, J_1^{-1}\right)$, where $J_1^{-1} \triangleq \mathrm{Tr}\left(\boldsymbol{J}_{\widetilde{\boldsymbol{\Theta}}}^{-1}\right) - 2\left[\boldsymbol{J}_{\widetilde{\boldsymbol{\Theta}}}^{-1}\right]_{(1,2)}$.

A proof is given in Appendix G.

Define $\beta_1 \triangleq \hat{D}_{p,a} - \hat{D}_{\mathrm{cov}}(p)$. Let $E_{p,a} = r$ and $E_{\mathrm{cov}} = r_0$. The FAR node can transmit with positive power, i.e., $s_a^* \neq -\infty$, if $0 < |r - r_0| < \beta_1$, otherwise $s_a^* = -\infty$ (see Fig. 3). Here, the critical distance from the FAR node is given by

$$d_a^* = d_{p,a} - d_{\mathrm{cov}}(p) = \hat{D}_{p,a} - r - (\hat{D}_{\mathrm{cov}}(p) - r_0) = \beta_1 - r_1,$$

where $r_1 \triangleq r - r_0$. We note that here r_1 plays the same role as r of Section IV-A. Similarly as before, for $s_a^* \neq -\infty$ we require $\beta_1 > \beta_1^* > 0$, where $\beta_1^* \triangleq \min\left\{\tilde{\beta}_1 : \Pr(|E_1| < \tilde{\beta}_1) \geq \varepsilon\right\} = \sqrt{J_1^{-1}} \cdot Q^{-1}\left(\frac{1-\varepsilon}{2}\right)$.

Analogous to Proposition 5, we obtain the following result for the case of unknown transmit power.

Proposition 7: For $|r_1| \leq 0.993\beta_1$, the interference probability conditioned on E_1 is upper bounded as follows:

$$P_{\mathrm{int}}(a, v | E_1 = r_1) \leq Q(b_1 + b_2|r_1|), \tag{48}$$

where b_1 and b_2 are given in (43).

The proof of Proposition 7 is similar to that of Proposition 5, which is given in Appendix E.

Integrating out r_1 in (48), we get

$$P_{\mathrm{int}}(a, v) \quad \leq \quad Q\left(\frac{b_1}{\sqrt{1 + b_2^2 J_1^{-1}}}\right), \tag{49}$$

which leads to an upper bound on the transmit power s_a by requiring the right-hand side of (49) to be less than $\varepsilon_{\mathrm{int}}$.

Similarly as before, for $s_a^* \neq -\infty$ we require $\beta_1 > \beta_1^* > 0$, where $\beta_1^* \triangleq \min\left\{\tilde{\beta}_1 : \Pr(|E_1| < \tilde{\beta}_1) \geq \varepsilon\right\} =$

$\sqrt{J_1^{-1}} \cdot Q^{-1}\left(\frac{1-\varepsilon}{2}\right)$. Finally, using the invariance principle we obtain the following approximation for the MIFTP:

$$\hat{s}_a = \begin{cases} i_{\text{max}} + 10\epsilon \log_{10} \beta_1 - \sigma_W \sqrt{1 + \left(\frac{50\epsilon}{\beta_1 \sigma_W \ln 10}\right)^2 \hat{J}_1^{-1}} \cdot Q^{-1}(\varepsilon_{\text{int}}), & \text{if } \beta_1 > \hat{\beta}_1^* > 0, \\ -\infty, & \text{otherwise,} \end{cases} \tag{50}$$

where $\hat{\beta}_1^* = \sqrt{\hat{J}_1^{-1}} \cdot Q^{-1}\left(\frac{1-\varepsilon}{2}\right)$.

V. Numerical Results

In this section, we present plots of the MIFTP and the approximate MIFTP estimated from SS measurements under a range of parameter settings. We choose our simulation parameters keeping in mind the application to unused digital television broadcast bands operating at the UHF band [37]. We consider two cases: i) the transmit power, s_p, of the primary node, p, is known and the FAR nodes only estimate the location $\boldsymbol{L}$, and ii) s_p is unknown and the FAR nodes estimate s_p along with $\boldsymbol{L}$. The crucial parameters affecting the MIFTP estimation are $d_{p,a}$, s_p, ε_{int}, σ_W, ϵ, N and the CRB $J_{p,a}^{-1}$. We shall assume that the remaining parameters are known constants. Each of the MIFTP values is calculated as an average over 1000 simulation trials and is shown with the associated 95% confidence interval. We set the parameters as follows:

- Detection thresholds for the victim and FAR nodes are $r_{\text{min}} = -83$ and $r_a = -121$ dBm, respectively.
- $\varepsilon_{\text{cov}} = 0.05$, $i_{\text{max}} = -100$ dBm, $\varepsilon_{\text{int}} = 0.01$.
- Standard deviation of shadowing noise, $\sigma_W = 8$ dB.
- Primary node location $\boldsymbol{L} = (50, 50)$ [km].

Five different scenarios are considered below.

A. Distance $d_{p,a}$

We vary $d_{p,a}$ from 20 to 100 km and position the target FAR node at $\boldsymbol{L}_a = (x_a, y_a)$, where

$$\boldsymbol{L}_a = \boldsymbol{L} + \frac{d_{p,a}}{\sqrt{2}}(1, 1). \tag{51}$$

For a given transmit power of the primary transmitter, $s_p = 80$ dBm, we find $d_{\text{det}}(a)$, the *detection distance* of the FAR nodes (cf. [16]). It denotes the radius beyond which the FAR nodes cannot detect the primary signal and is given by $d_{\text{det}}(a) = g^{-1}(s_p - r_a + \sigma_W Q^{-1}(1 - \varepsilon_{\text{cov}}))$, where r_a denotes the FAR node's detection threshold. The *detection region* of a FAR node a is the circular region centered at a with radius d_{det}.

For each simulation trial, we randomly place N FAR nodes, with uniform distribution, inside the circle with radius equal to $d_{\text{det}}(a)$ and centered at $\boldsymbol{L}$. The set of SS measurements to compute the MLE of $\boldsymbol{L}$ or $\boldsymbol{\Theta}$ is collected by these FAR nodes, which can be used by other FAR nodes further away to estimate their MIFTP values. The FAR

nodes estimate the MLE of $\boldsymbol{L}$ assuming a fixed path loss factor $\epsilon = 4$, which is a typical value for the shadowed urban cellular radio. Nodes lying outside $d_{\text{sense}}(a)$ use $\hat{\boldsymbol{L}}_{\text{ML}}$ or $\hat{\boldsymbol{\Theta}}_{\text{ML}}$ to estimate MIFTP based on (47) or (50). To find the ML location and transmit power estimates, we need to solve the following nonlinear optimization problem:

$$\hat{\boldsymbol{L}}_{\text{ML}} = \arg\max_{\boldsymbol{L}} f_{\boldsymbol{S}|\boldsymbol{L}} \qquad \text{or} \qquad \hat{\boldsymbol{\Theta}}_{\text{ML}} = \arg\max_{\boldsymbol{\Theta}} f_{\boldsymbol{S}|\boldsymbol{\Theta}}, \tag{52}$$

where $f_{\boldsymbol{S}|\boldsymbol{L}}$ and $f_{\boldsymbol{S}|\boldsymbol{\Theta}}$ denote the likelihood functions conditioned on $\boldsymbol{L}$ and $\boldsymbol{\Theta}$, respectively. To solve this we use the *fmincon* routine of Matlab®, which employs a sequential quadratic programming method. As the initial location estimate, we choose the midpoint of the rectangle that circumscribes the union of the detection regions of the FAR nodes making the SS measurements. The initial power estimate is set to 60 dBm. Alternatively, one could use the suboptimal estimates given in [38] as the initial starting point of the optimization problem.

Figs. 4(a) and 4(b) plot the true and estimated MIFTP values vs. $d_{p,a}$ for both known and unknown s_p when $N = 5, 10, 15, 20$. The confidence intervals shown in the plots arise due to randomness in the localizing FAR node positions, as well as the shadowing noise. We see that the accuracy of the approximate MIFTP formula improves with increasing $d_{p,a}$ and increasing N. When $\epsilon = 4$, roughly for $N \geq 10$, the performance degradation due to the estimation of s_p becomes negligible.

We can also calculate the probability of interference, $\hat{P}_{\text{int}}$, which results when the FAR node transmits with power level equal to the MIFTP estimate. Let $\hat{s}_a^i$ denote the MIFTP estimate for the ith simulation trial, $i = 1, \cdots, M$. Then the probability of interference under the MIFTP approximation is given by

$$\hat{P}_{\text{int}} = \frac{1}{M} \sum_{i=1}^{M} P_{\text{int}}(a|\hat{s}_a^i), \tag{53}$$

where $P_{\text{int}}(a|\hat{s}_a)$ denotes the interference probability given the FAR node transmit power $\hat{s}_a$ (cf. (9)).

Fig. 5 shows the plot of $\hat{P}_{\text{int}}$ versus $d_{p,a}$ for $\epsilon = 4$ when s_p is known. We observe that $\hat{P}_{\text{int}}$ increases with increasing $d_{p,a}$, but it is always less than ε_{int}. When s_p is unknown, $\hat{P}_{\text{int}}$ decreases further, since the MIFTP estimate becomes more conservative. In our simulations plotted in Figs. 6 and 7, we found that the MIFTP values depend strongly on the path loss factor ϵ. For larger values of ϵ, the accuracy of the MIFTP approximation improves significantly and the effect of N decreases. This is because, although the received signal becomes weaker as ϵ increases, the sensitivity of the MIFTP approximation on the location estimation error reduces. For $\epsilon = 5$, $\hat{P}_{\text{int}}$ increases as the MIFTP approximation becomes tighter, but always remains smaller than ε_{int}. Therefore, the approximate MIFTP can safely be used by the FAR node as an upper bound on the allowable transmit power.

B. Interference probability threshold, ε_{int}

In this scenario, we set $\epsilon = 4$, and $d_{p,a} = 50$ km. The location of the FAR node is set according to (51) and the values of the other parameters are set as in the previous scenario. For known s_p, Fig. 8(a) shows a plot of MIFTP vs. the interference probability threshold, ε_{int}, which is varied from 0.001 to 0.1. The same is repeated in Fig. 8(b) for the case of unknown s_p. We have also observed that the MIFTP increases relatively slowly with increasing ε_{int}. Also, the gap between the true and approximate MIFTP values decreases slowly with increasing ε_{int}. For $N \geq 10$, the performance degradation due to estimating the unknown s_p is negligible. We have observed that $\hat{P}_{\text{int}}$ increases almost linearly with increasing ε_{int}, but is always less than the specified threshold. From Figs. 8(a) and 8(b), we see that for $N \geq 10$, the MIFTP increases relatively slowly as ε_{int} increases. In particular, the difference between the MIFTP value when $\varepsilon_{\text{int}} = 0.001$ and when $\varepsilon_{\text{int}} = 0.1$ is about 15 dB.

C. Shadowing noise, σ_W

Here, we set $\varepsilon_{\text{int}} = 0.01$, keep all other parameters as before, and vary σ_W from 4 to 10 dB. From Figs. 9(a) and 9(b), we see that the MIFTP decreases almost linearly with increasing shadowing noise variance. The gap between the true and approximate MIFTP values does not depend strongly on the shadowing noise. Again, for $N \geq 10$, the performance degradation due to estimating the unknown s_p is negligible. We have also observed that $\hat{P}_{\text{int}}$ does not change appreciably with σ_W and is always less than ε_{int}.

D. Primary transmit power, s_p

Now, we set $\sigma_W = 8$ dB, and keep all other parameter values as before. Figs. 10(a) and 10(b) plot the true and approximate MIFTP values as s_p is varied from 20 to 80 dBm, for known and unknown s_p, respectively. We observe that the true MIFTP decreases by only a small amount. The accuracy of the approximate MIFTP formula falls off quickly with increasing s_p when $N \leq 5$. However, increasing N results in a significant improvement in MIFTP accuracy for high values of s_p. We have observed that $\hat{P}_{\text{int}}$ decreases with increasing s_p as the MIFTP approximation becomes looser and is always less than ε_{int}.

E. Cramér-Rao bound, $J_{p,a}^{-1}$

One of the crucial aspects of the MIFTP approximation is the use of the MLE of the CRB on position, $\hat{J}_{p,a}^{-1}$, instead of the true one, $J_{p,a}^{-1}$. Here, we look at the effect of this substitution by plotting in Fig. 11, the square root of $J_{p,a}^{-1}$ and the square root of its associated MLE $\hat{J}_{p,a}^{-1}$ as a function of σ_W for $N = 10, 15, 20$. As before, we fix $d_{p,a} = 50$ km and randomly place N localizing FAR nodes, with uniform distribution, inside the coverage circle of the primary transmitter and average over 1000 trials to obtain the performance metrics of interest. As expected,

with increasing N the CRB on location, $J_{p,a}^{-1}$, decreases, although the decrease is not significant for $N > 10$. This plot shows that the CRB does not depend strongly on σ_W in the chosen range. From the confidence intervals, we observe that the geometrical arrangement (i.e., the relative positions with respect to the primary transmitter) of the localizing nodes have only a small effect on the CRB estimation with known s_p for all N and with unknown s_p, when $N \geq 10$.

Another key observation is that in almost all cases, the MLE of the CRB is greater than its true value. This justifies the use of the estimated CRB in the MIFTP approximation formulas, since such overestimation of the true CRB ensures that the approximate MIFTP underestimates the true MIFTP. We have also plotted the CRB on the primary transmit power s_p, i.e., $\mathcal{E}_{\hat{S}_p}(\mathbf{\Theta})$, versus σ_W for $N = 10, 15, 20$. We observed that $\mathcal{E}_{\hat{S}_p}(\mathbf{\Theta})$ depends only weakly on σ_W and can be estimated quite accurately when $N \geq 10$.

F. Summary

The proposed MIFTP approximation performs well when a sufficient number of measurements is available. The accuracy of the approximation appears to be quite sensitive the value of the path loss factor. Increasing the number of measurements N significantly improves the accuracy and robustness of the MIFTP estimator. When $N = 10$ and s_p is known, we found that the MIFTP estimator is quite accurate over the entire range of parameter values that were used in the above scenarios. For $N \geq 10$, the estimation performance degradation due to unknown s_p and the effect of the localizing nodes' position with respect to the primary node is small. The plot of the CRB shows that the use of the invariance principle to estimate the true CRB is well justified. Finally, in all cases of our simulation studies, we found that the interference probability, $\hat{P}_{\text{int}}$, calculated using the MIFTP approximation is always less than the specified threshold ε_{int}.

VI. Multiple Co-channel Primary and Secondary Transmitters

In the previous sections we discussed in detail the proposed collaborative sensing and MIFTP estimation for successful opportunistic spectrum access. Our approach is to explicitly account for the error involved in the estimation process in order to avoid harmful interference to the primary system. We focused on the simple scenario where a single primary transmitter is being sensed by a cooperative FAR network, to determine the upper limit of interference-free transmit power of a single secondary transmitter. But for practical systems, one must consider the existence of multiple co-channel and potentially overlapping primary and secondary transmitters. This has two important implications for our opportunistic spectrum access scheme.

A. Multiple primary transmitters

A FAR node must guarantee interference-free transmission with respect to all the victim nodes located inside the coverage area of all the co-channel transmitters in the primary network. This can be accomplished by simply choosing the minimum of all the MIFTP values computed with respect to each of the primary transmitter individually. Hence, the MIFTP of the multiple primary transmitter case is straightforward if we know how to compute MIFTP for a single primary transmitter case.

As far as SS-based sensing is concerned, there is another important aspect. The co-channel interference of primary transmitters will introduce error in the SS measurements used to perform the sensing. Specifically, the total received SS S, due to M co-channel primary transmitters is given by

$$S \quad = \quad 10\log_{10}\left(\sum_{i=1}^{M} 10^{\frac{S_i}{10}}\right), \tag{54}$$

where S_i is the received SS due to the i^{th} primary transmitter, (cf. (16)).The fact that FAR nodes are likely to be more sensitive than typical primary receivers, can potentially make matters worse. Roughly speaking this is because, higher receiver sensitivity means larger *detection distance*, which means there will be a larger overlap region where FAR nodes can receive signal from multiple primary transmitters. The worst case scenario occurs when all the localizing FAR nodes are inside such an overlap region.

To provide some intuition on how the sensing accuracy is affected by multiple co-channel transmitters, we choose $M = 2$ with equal transmit power of 80 dBm for primary transmitters P_1 and P_2 and assume homogeneous propagation conditions. We consider two scenarios. In Fig. 12, the FAR nodes are uniformly distributed in the coverage area, and in Fig. 13, all the FAR nodes are located inside the overlap region A, which is the intersection area of the two *sensing circles* corresponding to primary transmitters P_1 and P_2. Region A represents the region most susceptible to error due to interference from the two transmitters. As a measure of error in localization, we use *error circles*, the mean of which is the mean estimate computed from 1000 trial runs and its radius is given by the corresponding CRB estimate. From Fig. 12 we see that the FAR nodes uniformly distributed around P_2 can successfully estimate $\hat{P}_2$ and the effect of interference from P_1 on localization accuracy is negligible. In Fig. 13, significant degradation is seen when FAR nodes are limited to region A. For $N = 10$ the effect of whether P_1 is present or not is small. But when $N = 20$, the gain in accuracy is limited by the presence of P_1. We note that for both Figs. 12 and 13, the true location of P_2 is always contained inside the *error circles*. To improve accuracy, especially in worst-case scenarios mentioned above, the error induced due to interference can be mitigated with additional information exchange and signal processing performed by the FAR nodes. A detailed treatment of this issue is the topic of our ongoing research and is beyond the scope of this paper.

B. Multiple secondary transmitters

If there are multiple FAR nodes willing to transmit, then the minimum of all the MIFTPs should be chosen and allocated among the aspiring FAR nodes using a network layer protocol. Given that a FAR node has prior knowledge about the estimated locations and transmit powers of other cochannel transmitting FAR nodes, a FAR node can simply treat them as primary transmitters to avoid secondary-secondary interference.

VII. Conclusion

The main result of this paper is an approximate formula for the maximum interference-free transmit power (MIFTP), which a FAR can use in a given frequency channel without causing harmful interference to victim nodes. The approximate MIFTP formula relies on location and transmit power estimates derived from signal strength measurements obtained by one or more FAR nodes in the vicinity of a given primary transmitter. In effect, the MIFTP provides a concrete characterization of the size of the spectrum hole in the spatial domain and can be applied directly to opportunistic spectrum access mechanisms.

Our numerical results validate the accuracy of the proposed MIFTP estimation formula for several different scenarios and over a range of parameter settings. The proposed scheme for spectrum hole estimation can be used to significantly enhance the performance of spectrum access methods, such as the Listen-Before-Talk (LBT) scheme [16], by exploiting collaboration among the FAR nodes. Although we focused on the scenario of a signal primary transmitter, our approach could be extended to handle the more general case of multiple simultaneous primary and secondary transmitters, as discussed in Section VI. A full treatment of this case is deferred to a forthcoming paper. In ongoing work, we are also exploring how other types of information gathered by collaborative FAR nodes can be used to further improve the efficiency of spectrum hole estimation.

References

[1] M. McHenry, "Frequency agile spectrum access technologies," in *Proc. FCC Workshop on Cognitive Radio*, May 2003.

[2] G. Staple and K. Werbach, "The end of spectrum scarcity," *IEEE Spectrum*, vol. 41, pp. 48–52, March 2004.

[3] S. Haykin, "Cognitive radio: Brain-empowered wireless communications," *IEEE J. Selected Areas in Comm.*, vol. 23, pp. 201–220, Feb. 2005.

[4] J. Mitola *et al.*, "Cognitive radio: Making software radios more personal," *IEEE Pers. Commun.*, vol. 6, pp. 13–18, Aug. 1999.

[5] J. M. Peha, "Approaches to spectrum sharing," *IEEE Communications Magazine*, vol. 43, pp. 10–12, Feb. 2005.

[6] N. Devroye, P. Mitran, and V. Tarokh, "Limits on communications in a cognitive radio channel," *IEEE Communications Magazine*, vol. 44, pp. 44–49, June 2006.

[7] S. M. Mishra, A. Sahai, and R. W. Brodersen, "Cooperative sensing among cognitive radios," in *IEEE Int. Conf. on Comm.*, vol. 4, pp. 1658–1663, June 2006.

[8] G. Ganesan and Y. Li, "Cooperative spectrum sensing in cognitive radio networks," in *Proc. IEEE Int. Symp. on New Frontiers in Dynamic Spectrum Access Networks (DySPAN)*, pp. 137–143, Nov. 2005.

[9] A. Jovicic and P. Viswanath, "Cognitive radio: An information-theoretic perspective," in *Proc. IEEE Int. Symp. on Information Theory*, pp. 2413–2417, July 2006.

[10] M. Gastpar, "On capacity under receive and spatial spectrum-sharing constraints," *IEEE Trans. on Information Theory*, vol. 53, pp. 471–487, Feb. 2007.

[11] A. Ghasemi and E. S. Sousa, "Fundamental limits of spectrum-sharing in fading environments," *IEEE Trans. on Wireless Comm.*, vol. 6, pp. 649–658, Feb. 2007.

[12] R. Etkin, A. Parekh, and D. Tse, "Spectrum sharing for unlicensed bands," in *Proc. IEEE Int. Symp. on New Frontiers in Dynamic Spectrum Access Networks (DySPAN)*, pp. 251–258, Nov. 2005.

[13] D. Cabric, I. O'Donnell, M.-W. Chen, and R. Brodersen, "Spectrum sharing radios," *IEEE Circuits and Systems Magazine*, vol. 6, pp. 30–45, Feb. 2006.

[14] R. Menon, R. M. Buehrer, and J. H. Reed, "Outage probability based comparison of underlay and overlay spectrum sharing techniques," in *Proc. IEEE DySPAN*, pp. 101–109, Nov. 2005.

[15] N. Hoven and A. Sahai, "Power scaling for cognitive radio," in *Proc. Int. Conf. on Wireless Networks, Communications and Mobile Computing*, pp. 250–255, June 2005.

[16] A. E. Leu, M. McHenry, and B. L. Mark, "Modeling and analysis of interference in Listen-Before-Talk spectrum access schemes," *Int. J. Network Mgmt*, vol. 16, pp. 131–147, 2006.

[17] S. Tang and B. L. Mark, "Performance analysis of a wireless network with opportunistic spectrum sharing," in *Proc. IEEE Globecom*, (Washington DC), Nov. 2007.

[18] Q. Zhao and A. Swami, "A decision-theoretic framework for opportunistic spectrum access," *IEEE Communications Magazine: Special Issue on Cognitive Wireless Networks*, vol. 14, pp. 14–20, Aug. 2007.

[19] S. Capkun, M. Hamdi, and J.-P. Hubaux, "GPS-Free positioning in mobile ad-hoc networks," in *Proc. 34th Hawaii Int. Conf. System Sciences*, Jan. 2001.

[20] D. Moore, J. Leonard, D. Rus, and S. Teller, "Robust distributed network localization with noisy range measurements," in *Proc. 2nd ACM SenSys*, Nov. 2004.

[21] P. Biswas and Y. Ye, "Semidefinite programming for ad hoc wireless sensor network localization," in *3rd Int. Symp. on Information Processing in Sensor Networks, IPSN 2004*, pp. 46–54, April 2004.

[22] L. Doherty, K. S. J. Pister, and L. E. Ghaoui, "Convex position estimation in wireless sensor networks," in *Proc. IEEE INFOCOM'01*, vol. 3, pp. 1655–1663, April 2001.

[23] M. Gudmundson, "Correlation model for shadow fading in mobile radio systems," *Electronics Letters*, vol. 47, pp. 2145–2146, Nov. 1991.

[24] M. N. Lustgarten and J. A. Madsen, "An empirical propagation model (EPM-73)," *IEEE Trans. on Electromagnetic Compatibility*, vol. 19, August 1977.

[25] A. G. Longley and P. L. Rice, "Prediction of tropospheric transmission loss over irregular terrain, a computer method - 1968," ESSA 79-ITSS 67, U.S. Dept. of Commerce, Office of Telecommunications, Boulder, CO, July 1968.

[26] N. S. Adawi *et al.*, "Coverage prediction for mobile radio systems operating in the 800/900 MHz frequency range," *IEEE Trans. on Vehicular Technology*, vol. 37, pp. 3–44, 1988.

[27] Y. Qi, H. Kobayashi, and H. Suda, "Analysis of wireless geolocation in a non-line-of-sight environment," *IEEE Trans. on Wireless Comm.*, vol. 5, pp. 672–681, March 2006.

[28] J. J. Caffery, *Wireless Location in CDMA Cellular Radio Systems*. Massachusetts: Kluwer Academic Publishers, 1999.

[29] Y. Qi, *Wireless geolocation in a non-line-of-sight environment*. PhD thesis, Princeton University, Princeton, New Jersey, 2003.

[30] A. J. Weiss, "On the accuracy of a cellular location system based on RSS measurements," *IEEE Trans. on Vehicular Tech.*, vol. 52, pp. 1508–1518, Nov. 2003.

[31] V. Erceg *et al.*, "An empirically based path loss model for wireless channels in suburban environment," *IEEE J. Selected Areas in Comm.*, vol. 17, pp. 1205–1211, July 1999.

[32] C. Pérez-Vega and J. M. Zamanillo, "Path-loss model for broadcasting applications and outdoor communication systems in the VHF and UHF bands," *IEEE Trans. on Broadcasting*, vol. 48, pp. 91–96, June 2002.

[33] C. R. Rao, *Linear Statistical Inference and Its Applications*. New York: John Wiley & Sons, Inc., 2 ed., 1965.

[34] L. L. Scharf, *Statistical Signal Processing: Detection, Estimation, and Time Series Analysis*. New York: Addison-Wesley, 1991.

[35] H. L. Van Trees, *Detection, Estimation and Modulation Theory: Part I*. New York: John Wiley & Sons, Inc., paperback ed., 2001.

[36] S. Verdú, *Multiuser Detection*. New York: Cambridge University Press, 1998.

[37] "Longley-Rice Methodology for evaluating TV coverage and Interference.," Tech. Rep. OET Bulletin 69, Office of Engineering and Technology (OET), Federal Communications Commission, Feb. 2004.

[38] S. Kim, H. Jeon, and J. Ma, "Robust localization with unknown transmission power for cognitive radio," in *Proc. IEEE Int. Conf. on Military Communications*, Oct. 2007.

APPENDIX

A. Proof of Proposition 2

The score function $\frac{\partial}{\partial \boldsymbol{\Theta}} \ln f_{\boldsymbol{S}|\boldsymbol{\Theta}}(\boldsymbol{S})$ can be expressed as

$$\frac{\partial}{\partial \boldsymbol{\Theta}} \ln f_{\boldsymbol{S}|\boldsymbol{\Theta}}(\boldsymbol{S}) = \frac{1}{\sigma_W^2} \boldsymbol{BGDW}, \tag{55}$$

where $\boldsymbol{B}$ is given by (30) and $\boldsymbol{D}$ is given by (25). So the FIM is given by

$$\boldsymbol{J}_{\boldsymbol{\Theta}} = \frac{1}{\sigma_W^4} E_{\boldsymbol{\Theta}} \left[\boldsymbol{BGDW} (\boldsymbol{BGDW})^T \right] = \frac{1}{\sigma_W^4} \boldsymbol{BGD} \cdot E[\boldsymbol{WW}^T] \cdot \boldsymbol{DG}^T \boldsymbol{B} = \frac{1}{\sigma_W^2} \boldsymbol{BGD}^2 \boldsymbol{G}^T \boldsymbol{B}. \tag{56}$$

B. Proof of Proposition 3

Differentiating z_i with respect to $\boldsymbol{\Theta} = [x_p, y_p, s_p]^T$, we obtain

$$\frac{\partial z_i}{\partial \boldsymbol{\Theta}} = \left[\frac{-10\epsilon \cos \phi_i}{d_i \ln 10}, \frac{-10\epsilon \sin \phi_i}{d_i \ln 10}, 1 \right]^T. \tag{57}$$

Hence,

$$\frac{\partial \boldsymbol{z}}{\partial \boldsymbol{\Theta}} = \boldsymbol{BGD}. \tag{58}$$

Let $\Delta\boldsymbol{\Theta} \triangleq \hat{\boldsymbol{\Theta}} - \boldsymbol{\Theta}$. Then for sufficiently small $|\Delta\boldsymbol{\Theta}|$, we can write

$$\Delta \boldsymbol{z} \approx (\boldsymbol{BDG})^T \Delta\boldsymbol{\Theta}, \tag{59}$$

where $\Delta \boldsymbol{z} = \hat{\boldsymbol{z}} - \boldsymbol{z}$, and $\hat{\boldsymbol{z}}$ is an estimate of $\boldsymbol{z}$. Under the assumption that the variance of W_i is sufficiently small, Δz_i can be interpreted as the error in the SS estimate S_i. Hence, $\boldsymbol{S} = \hat{\boldsymbol{z}}$, which implies that for sufficiently small

σ_W^2, $\Delta \boldsymbol{z} = \boldsymbol{S} - \boldsymbol{z} = \boldsymbol{W}$, and under this condition, (59) can be written as

$$\boldsymbol{S} - \boldsymbol{z} = \boldsymbol{W} = (\boldsymbol{BDG})^T(\hat{\boldsymbol{\Theta}} - \boldsymbol{\Theta}). \tag{60}$$

The conditional pdf $f_{\boldsymbol{S}|\boldsymbol{\Theta}}(\boldsymbol{S})$ has the form of a multivariate Gaussian distribution:

$$f_{\boldsymbol{S}|\boldsymbol{\Theta}}(\boldsymbol{S}) \propto \exp\left\{-\frac{1}{2}(\boldsymbol{S} - \boldsymbol{z})^T \boldsymbol{\Lambda}^{-1}(\boldsymbol{S} - \boldsymbol{z})\right\}, \tag{61}$$

where $\boldsymbol{\Lambda} = \sigma_W^2 \boldsymbol{I}$ and $\boldsymbol{I}$ is the $N \times N$ identity matrix. Substituting (60) into (61), we obtain (37).

C. Derivation of (38)

Using (58) and (60), we have

$$\frac{\partial}{\partial \boldsymbol{\Theta}} \ln f_{\boldsymbol{S}|\boldsymbol{\Theta}}(\boldsymbol{S}) = \frac{\partial \boldsymbol{z}}{\partial \boldsymbol{\Theta}} \cdot \frac{\partial}{\partial \boldsymbol{z}} \ln f_{\boldsymbol{S}|\boldsymbol{\Theta}}(\boldsymbol{S}) = \boldsymbol{BGD} \cdot \boldsymbol{\Lambda}^{-1}(\boldsymbol{S} - \boldsymbol{z}) = \boldsymbol{J}_{\boldsymbol{\Theta}}(\hat{\boldsymbol{\Theta}} - \boldsymbol{\Theta}).$$

D. Proof of Proposition 4

Let $\theta \triangleq d_{p,a}$ denote the true distance between the primary transmitter and the FAR node. The observation equation for estimating θ is given by

$$\hat{\boldsymbol{L}} = \boldsymbol{u} + \boldsymbol{W}_{\boldsymbol{L}}, \tag{62}$$

where $\boldsymbol{u} = [u_1, u_2]^T$ with

$$u_1 = x_a + \theta \cos\phi_{p,a} \text{ and } u_2 = y_a + \theta \sin\phi_{p,a},$$

and $\boldsymbol{W}_{\boldsymbol{L}} \sim \mathcal{N}(\boldsymbol{0}, \boldsymbol{J}_{\boldsymbol{L}}^{-1})$. Differentiating $\boldsymbol{u}$ with respect to θ, we have

$$\frac{\partial \boldsymbol{u}}{\partial \theta} = [\cos\phi_{p,a}, \ \sin\phi_{p,a}] = \boldsymbol{H}_{p,a}^T. \tag{63}$$

Let $\Delta\theta = \hat{\theta} - \theta$, where $\hat{\theta} \triangleq \hat{D}_{p,a}$. For sufficiently small $|\Delta\theta|$, we can write

$$\Delta \boldsymbol{u} \approx \boldsymbol{H}_{p,a} \Delta\theta. \tag{64}$$

Assuming that σ_W is small, $\Delta\boldsymbol{u}$ can be interpreted as the error in the location estimate $\hat{\boldsymbol{L}}$, in which case

$$\hat{\boldsymbol{L}} - \boldsymbol{u} = \boldsymbol{W}_{\boldsymbol{L}} = \boldsymbol{H}_{p,a}(\hat{\theta} - \theta). \tag{65}$$

Hence,

$$f_{\hat{\boldsymbol{L}}|\theta}(\hat{\boldsymbol{L}}) \propto \exp\left\{-\frac{1}{2}(\hat{\boldsymbol{L}} - \boldsymbol{u})^T \boldsymbol{J}_{\boldsymbol{L}}(\hat{\boldsymbol{L}} - \boldsymbol{u})\right\} = \exp\left\{-\frac{1}{2}(\hat{\theta} - \theta)^T \boldsymbol{H}_{p,a}^T \boldsymbol{J}_{\boldsymbol{L}} \boldsymbol{H}_{p,a}(\hat{\theta} - \theta)\right\}, \tag{66}$$

which implies that $E[\hat{\theta}] = \theta$. Hence $\hat{\theta}$ is unbiased in the asymptotic regime $\sigma_W \to 0$. In the asymptotic regime, the score function is

$$\frac{\partial}{\partial \theta} \ln f_{\hat{\boldsymbol{L}}|\theta}(\hat{\boldsymbol{L}}) = \boldsymbol{H}_{p,a}^T \boldsymbol{J}_{\boldsymbol{L}} \boldsymbol{H}_{p,a}(\hat{\theta} - \theta) = J_{p,a}(\hat{\theta} - \theta). \tag{67}$$

The last equality (see [34], p. 230) allows us to conclude that the CRB is achieved by the MLE $\hat{\theta} = \hat{D}_{p,a}$. From (66) and (67), it can be seen that in the asymptotic regime $E_{p,a} \sim \mathcal{N}(0, J_{p,a}^{-1})$.

E. Proof of Proposition 5

First, we prove the proposition for the case $r \geq 0$.

$$P_{\text{int}}(a, v|E_{p,a} = r) = \Pr\{I_v \geq i_{\max}|E_{p,a} = r\} \leq \Pr\{W \geq i_{\max} + g(d_a^*) - s_a|E_{p,a} = r\} \tag{68}$$

$$= Q\left(\frac{i_{\max} + 10\epsilon \log_{10} d_a^* - s_a}{\sigma_W}\right) = Q\left(\frac{i_{\max} + \frac{10\epsilon}{\ln 10}\ln(\beta - r) - s_a}{\sigma_W}\right). \tag{69}$$

We expand $\ln(\beta - r)$ in a Taylor series and lower bound it as follows:

$$\ln(\beta - r) = \ln\beta - \sum_{i=1}^{\infty} \frac{1}{i}\left(\frac{r}{\beta}\right)^i \geq \ln\beta - \frac{kr}{\beta},$$

for $0 \leq \frac{r}{\beta} \leq t_k < 1$, where t_k denotes the root of the function $f(t) = \ln(1-t) + kt$ near 1 with $t \in [0, 1)$ and $k > 0$. The value of t_k can be chosen arbitrarily close to one, for example, when $k = 5$, we have $t_k = 0.993$. Hence, we can write

$$P_{\text{int}}(a, v|E_{p,a} = r) \leq Q\left(\frac{i_{\max} + \frac{10\epsilon}{\ln 10}\left(\ln\beta - \frac{5r}{\beta}\right) - s_a}{\sigma_W}\right) = Q(b_1 + b_2 r).$$

Similarly, for $r < 0$ we can write

$$P_{\text{int}}(a, v|E_{p,a} = r) < Q\left(\frac{i_{\max} + \frac{10\epsilon}{\ln 10}\ln(\beta + r) - s_a}{\sigma_W}\right).$$

Again, using Taylor series expansion we can lower bound $\ln(\beta + r)$ as follows:

$$\ln(\beta + r) = \ln\beta + \sum_{i=1}^{\infty} \frac{(-1)^{i+1}}{i}\left(\frac{r}{\beta}\right)^i \geq \ln\beta + \frac{kr}{\beta},$$

for $-1 < t_k \leq \frac{r}{\beta} < 0$, where t_k denotes the root of the function $f(t) = \ln(1+t) - kt$ near -1 with $t \in (-1, 0)$ and $k > 0$. Like before, t_k can be chosen arbitrarily close to -1, for example, when $k = 5$, we have $t_k = -0.993$. Therefore, for $r < 0$, we can write

$$P_{\text{int}}\left(a, v \mid E_{p,a} = r\right) < Q\left(\frac{i_{\max} + \frac{10\epsilon}{\ln 10}\ln\left(\beta + \frac{5r}{\beta}\right) - s_a}{\sigma_W}\right) = Q(b_1 - b_2 r).$$

F. Derivation of (46)

Since $E_{p,a} \sim \mathcal{N}(0, J_{p,a}^{-1})$, we can evaluate $\Pr(|E_{p,a}| < \tilde{\beta})$ as follows.

$$\Pr(|E_{p,a}| < \tilde{\beta}) \quad = \quad \int_{-\tilde{\beta}}^{\tilde{\beta}} f_{E_{p,a}}(r)dr = 1 - 2Q\left(\frac{\tilde{\beta}}{\sqrt{J_{p,a}^{-1}}}\right). \tag{70}$$

We can find β^* by solving for the minimum value of $\tilde{\beta}$ such that $\Pr(|E_{p,a}| < \tilde{\beta}) \geq \varepsilon$ is satisfied. Using (70), this condition implies

$$\beta^* \quad = \quad \sqrt{J_{p,a}^{-1}} \cdot Q^{-1}\left(\frac{1-\varepsilon}{2}\right). \tag{71}$$

G. Proof of Proposition 6

Since we have two parameters $\boldsymbol{\Theta}$ and $\widetilde{\boldsymbol{\Theta}}$, where $\widetilde{\boldsymbol{\Theta}}$ is a function of $\boldsymbol{\Theta}$, then there exists a simple transformation (under some regularity conditions) relating their associated CRBs, $\boldsymbol{J}_{\boldsymbol{\Theta}}^{-1}$ and $\boldsymbol{J}_{\widetilde{\boldsymbol{\Theta}}}^{-1}$, [34] p. 229. Particularly,

$$\boldsymbol{J}_{\widetilde{\boldsymbol{\Theta}}}^{-1} \quad = \quad \boldsymbol{H}_1^T \boldsymbol{J}_{\boldsymbol{\Theta}}^{-1} \boldsymbol{H}_1 \tag{72}$$

where

$$\boldsymbol{H}_1 \quad \triangleq \quad \begin{bmatrix} \cos\phi_{p,a} & 0 \\ \sin\phi_{p,a} & 0 \\ 0 & \frac{\ln 10}{10\epsilon} d_{\text{cov}}(p) \end{bmatrix}. \tag{73}$$

Recall from Section III-C that the MLE, $\hat{\boldsymbol{\Theta}}_{\text{ML}}$, achieves the CRB asymptotically as $\sigma_W^2 \to 0$. Then, using similar arguments to Proposition 4, we can conclude that in the asymptotic regime, $\hat{\widetilde{\boldsymbol{\Theta}}}_{\text{ML}}$ also achieves its corresponding CRB. This means that for vanishingly small noise, E_1 can be modeled as $E_1 \sim \mathcal{N}(0, J_1^{-1})$, where J_1^{-1} can be computed as follows.

$$J_1^{-1} \quad = \quad E\left[E_{p,a} - E_{\text{cov}}\right]^2 \tag{74}$$

$$\quad = \quad E\left[E_{p,a}^2 + E_{\text{cov}}^2 - 2E_{p,a}E_{\text{cov}}\right] \tag{75}$$

$$\quad = \quad \text{Tr}\left(\boldsymbol{J}_{\widetilde{\boldsymbol{\Theta}}}^{-1}\right) - 2\left[\boldsymbol{J}_{\widetilde{\boldsymbol{\Theta}}}^{-1}\right]_{(1,2)}. \tag{76}$$

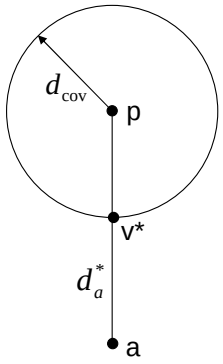

Fig. 1. FAR node a outside coverage area of primary transmitter p.

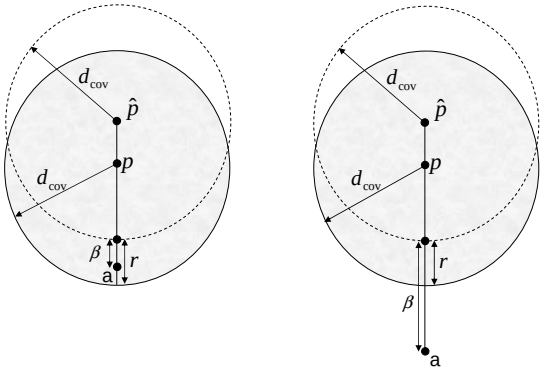

(a) $|r| > \beta$ (b) $|r| < \beta$

Fig. 2. Illustration of relationship between r and β. If $0 < |r| < \beta$, $s_a^* \neq -\infty$. Otherwise, $s_a^* = -\infty$.

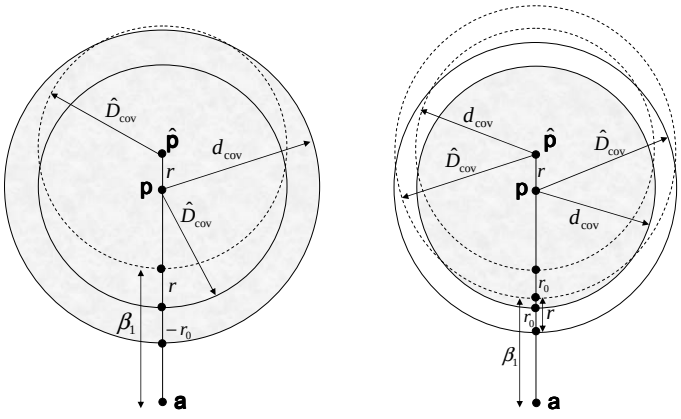

(a) $r_0 = \hat{D}_{\text{cov}} - d_{\text{cov}} < 0$ (b) $r_0 = \hat{D}_{\text{cov}} - d_{\text{cov}} > 0$

Fig. 3. Illustration of relationship between r, r_0, and β. In both cases, $0 < |r - r_0| < \beta_1$, which implies that $s_a^* \neq -\infty$.

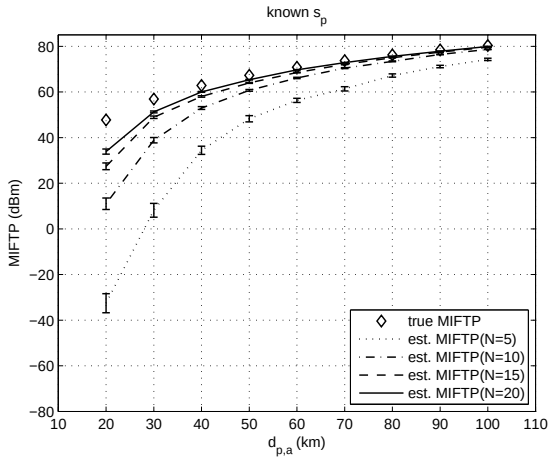

(a) s_p is known.

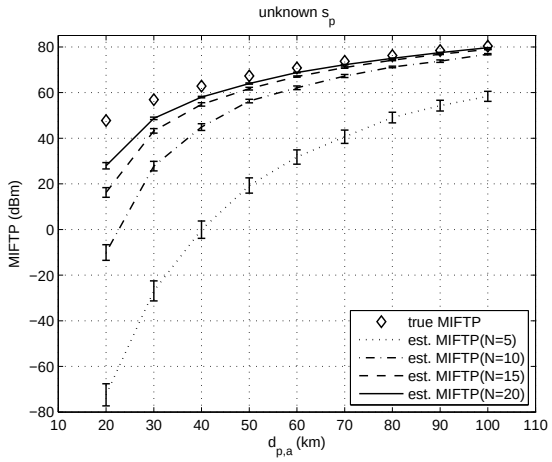

(b) s_p is unknown.

Fig. 4. MIFTP versus $d_{p,a}$, when $\epsilon = 4$.

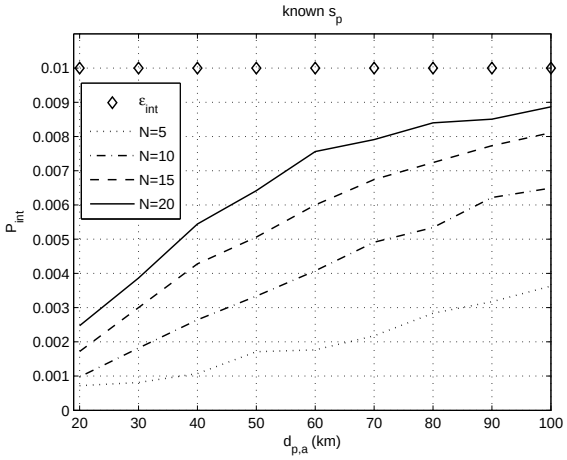

Fig. 5. $\hat{P}_{\text{int}}$ versus $d_{p,a}$, when $\epsilon = 4$ and s_p is known.

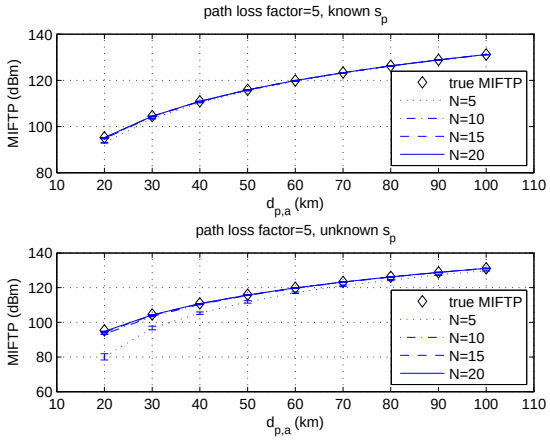

Fig. 6. MIFTP versus $d_{p,a}$, when $\epsilon = 5$.

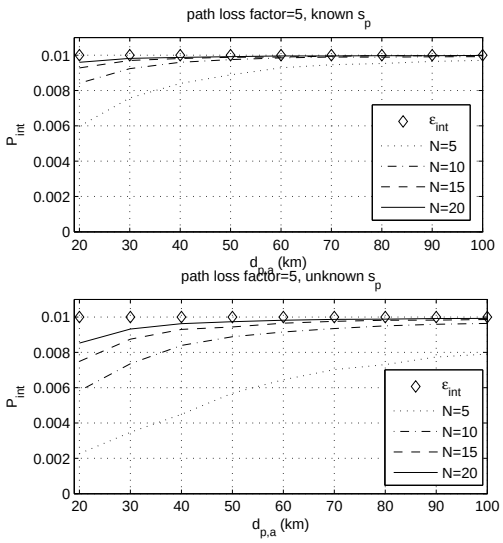

Fig. 7. $\hat{P}_{\text{int}}$ versus $d_{p,a}$, when $\epsilon = 5$.

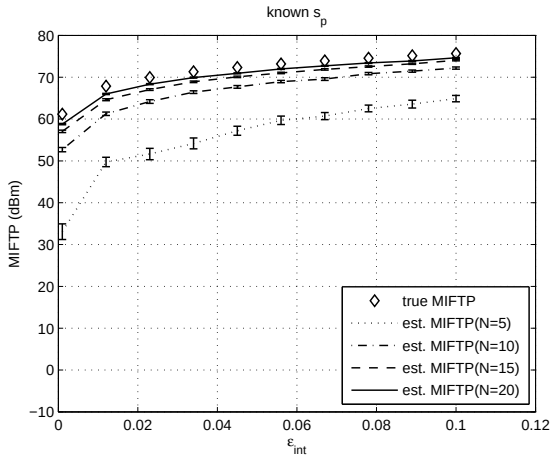

(a) s_p is known.

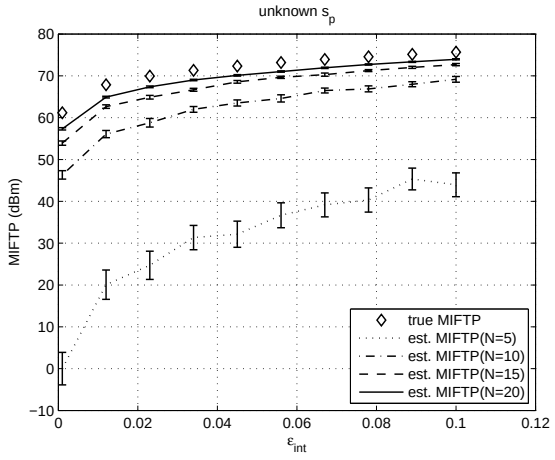

(b) s_p is unknown.

Fig. 8. MIFTP versus ε_{int}, when $\epsilon = 4$.

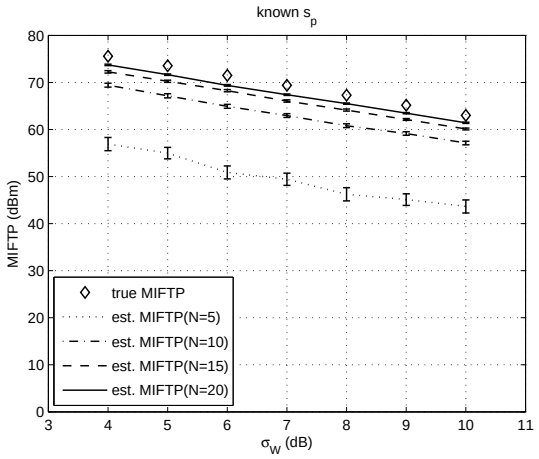

(a) s_p is known.

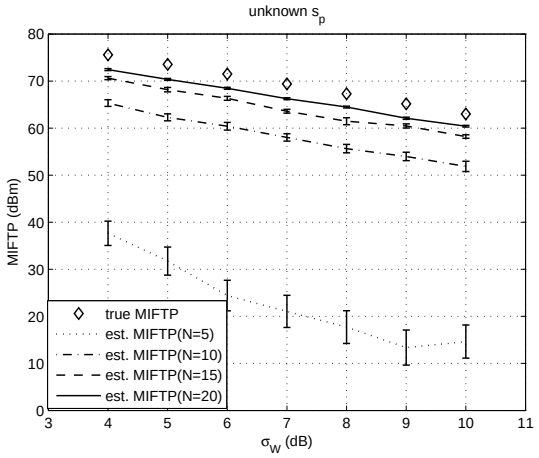

(b) s_p is unknown.

Fig. 9. MIFTP versus σ_W, when $\epsilon = 4$.

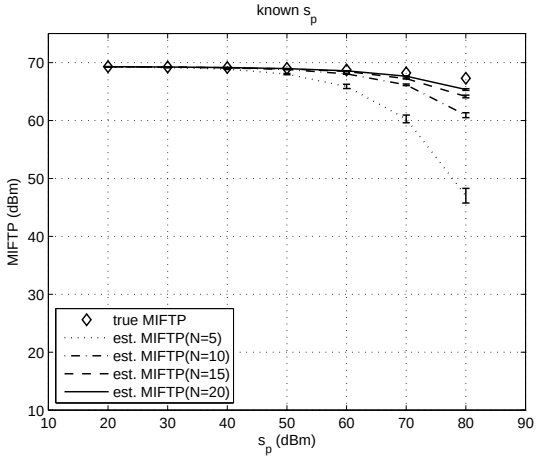

(a) s_p is known.

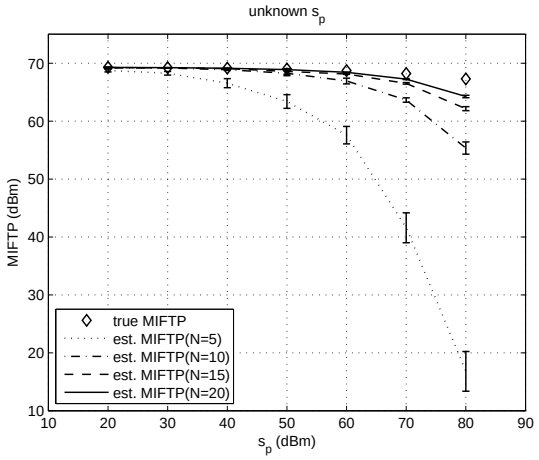

(b) s_p is unknown.

Fig. 10. MIFTP versus s_p, when $\epsilon = 4$.

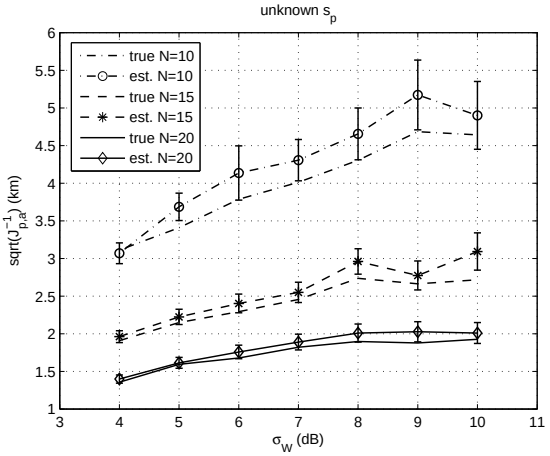

Fig. 11. $\sqrt{J_{p,a}^{-1}}$ versus σ_W, when $\epsilon = 4$ and s_p is unknown.

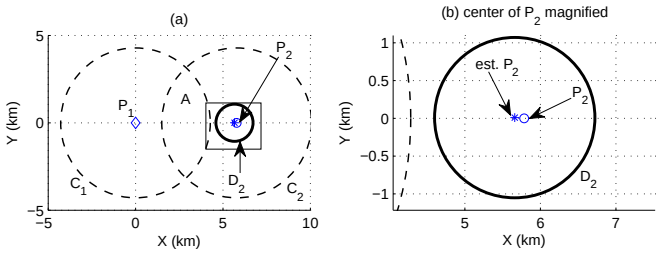

Fig. 12. In (a), circles C_1 and C_2 (dashed line) denote the *sensing distance* for primary transmitters P_1 and P_2, respectively. Region A is the overlap region of C_1 and C_2, and it denotes the area where FAR nodes are most likely to receive misleading SS measurements due to interfering transmitters. Circle D_2 (solid line) denotes the *error circle* which quantifies the localization error of P_2 when $N = 10$ and FAR nodes are uniformly distributed in C_2. The mean of D_2 is the mean estimate computed from 1000 trial runs and its radius is given by the corresponding CRB estimate. A magnified version of the center of P_2 in (a) is shown in (b). Nodes uniformly distributed around P_2 can successfully estimate $\hat{P}_2$ and the effect of interference from P_1 on localization accuracy is negligible.

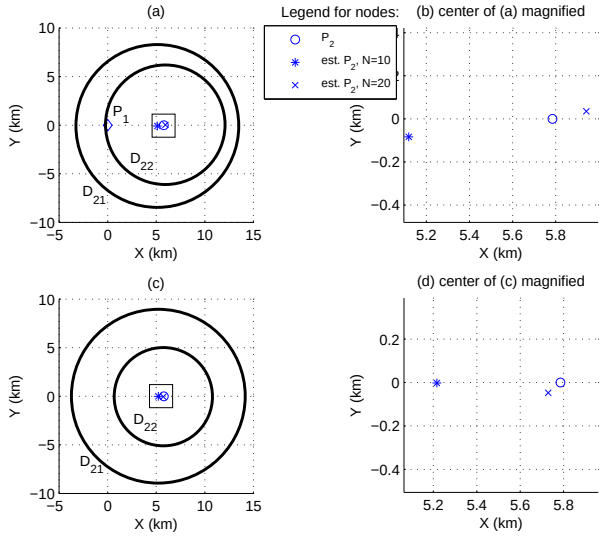

Fig. 13. All localizing nodes are placed inside region A (not shown). In (a), the two *error circles* D_{21} and D_{22} (solid line) correspond to localization error of P_2 when P_1 is present for $N = 10$ and $N = 20$, respectively. For comparison, (c) is included, where P_1 is absent. A magnified version of the center of P_2 in (a) and (c) are shown in (b) and (d), respectively.